A CMOD-Based Hybrid Approach to Determine Fracture Resistance Curve

Wuchao Yang[1], Xudong Qian[1,*]

[1] Department of Civil and Environmental Engineering, National University of Singapore, Singapore 117576, Singapore
* Corresponding author: qianxudong@nus.edu.sg

Abstract This study proposes a hybrid approach that relies both on the numerically computed and on the experimentally measured load (P) versus the crack-mouth opening displacement (CMOD) relationships to derive the fracture resistance curve (J-R curve) for the mixed-mode I and II fracture specimen. The CMOD-based hybrid approach utilizes a single experimental specimen with a growing crack and multiple finite element (FE) models, each with a different crack depth. The experimental procedure measures the P-CMOD curve from a standard fracture specimen with a growing crack. The intersections between the experimental P-CMOD curve and the numerical P-CMOD curves from multiple FE models dictate the CMOD levels to compute the strain energy (U). This approach simplifies the J-R curve test for the single-edge-notched bend, SE(B), specimen by eliminating the multiple unloading and reloading procedures in determining the variation of the compliance during the test. This method also provides an alternative simple measurement of the J-R curves for mixed-mode I and II specimens. The validation procedure shows accurate predictions of the J-R curves for both SE(B) specimens and mixed-mode I and II specimens.

Keywords mixed-mode fracture, fracture resistance, J-R curve, hybrid approach.

1. Introduction

The traditional load-line displacement (LLD) based incremental method has become widely implemented as a convenient experimental method to determine the fracture resistance curve, namely the J-R curve, for the SE(B) specimen, as recommended by the testing standards [1, 2]. The measurement of the specimen compliance at the each unloading and reloading procedure leads to a direct evaluation of the crack extension (Δa). The area under the load versus the LLD curve corresponding to different crack lengths allows the calculation of the energy release rate, J-value [3]. However, the measurement of the LLD for the SE(B) specimen requires extreme effort to prevent the potential errors introduced by the indentation at the loading point and the deformation of the testing frame [4]. In addition, the fracture toughness tests for the mixed-mode I and II specimens face critical challenges such as the calculation of the J-value and the determination of Δa [5]. The evaluation of the bending strain energy, which contributes to the J-value, depends on the current crack size (a_i) which cannot be determined via the traditional compliance approach for mixed-mode I and II specimens due to the unknown crack path prior to the test. Therefore, the experimental determination of the fracture resistance curve for both pure mode I SE(B) specimen and the mixed-mode I and II specimen requires a simplified and accurate approach based on the readily measurable quantities from the tests.

This study proposes a hybrid, numerical and experimental approach to determine the fracture resistance curve based on the readily measureable load versus CMOD (or Δ) relationship for SE(B) specimen (CMOD-hybrid approach). This research also extends the same approach to determine the fracture resistance for the mixed-mode I and II specimens. The J-value is derived from the variation in the total strain energy (including the bending and shear strain energy) with respect to the change in the crack depth, using the P-Δ curve measured from a single experimental specimen and P-Δ curves computed from multiple FE models with different crack sizes. The comparison of the fracture resistance curve obtained using the CMOD-hybrid approach with those obtained from the experimental results for both the SE(B) specimens and mixed-mode I and II specimens confirms the accuracy of the proposed CMOD-hybrid approach.

2. The CMOD-Based Hybrid Approach

The fundamental principle underlying the hybrid numerical and experimental approach remains similar to that of the conventional, multiple-specimen experimental approach proposed by Begley and Landes [6]. The procedure in the CMOD-hybrid approach follows similarly the hybrid approach, which relies on the *P*-LLD relations, proposed by the authors [7, 8], as illustrated in Figure 1. The numerical analyses of the hybrid approach generate a series of *P*-Δ curves from large-deformation, elastic-plastic analyses of multiple FE specimens with the same geometry, dimension and material, but different crack sizes. The experimental part of the hybrid approach produces the *P*-Δ curve for a fracture specimen with a growing crack.

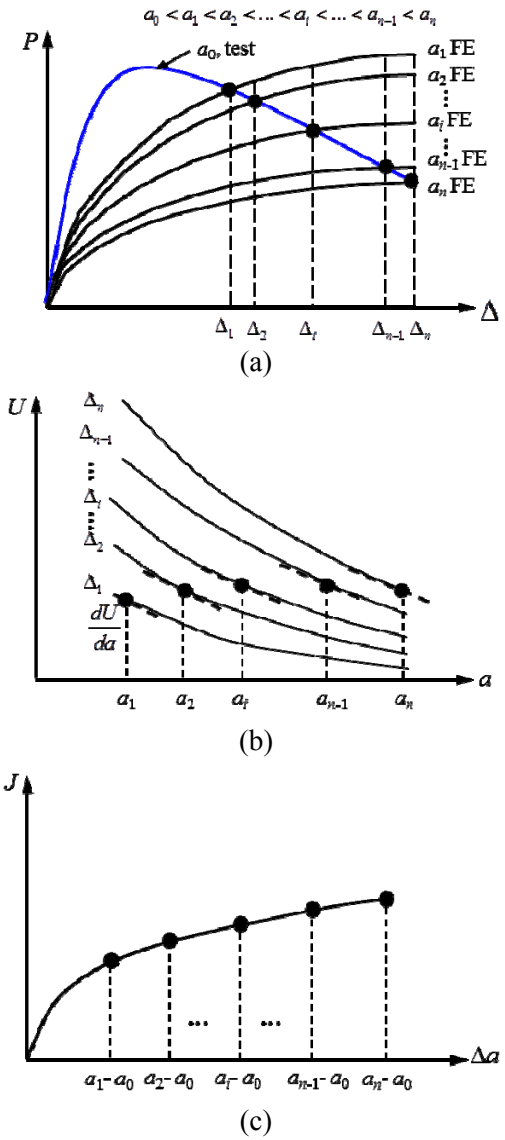

Figure 1. Schematic description for the proposed CMOD-based hybrid approach to determine the ductile fracture resistance.

Figure 1a illustrates the *P*-Δ curve obtained from the experimental specimen with the initial crack depth of a_0 and those obtained from the FE models with crack sizes ranging from a_1 to a_n. The intersection point between the experimental *P*-Δ curve and the numerical *P*-Δ curve defines a common loading and CMOD level in the FE specimen with a stationary crack and the experimental specimen with a growing crack. The crack extension (Δa_i) in the experimental specimen assumes a

value of ($a_i - a_0$) at the intersection of the test P-Δ curve and the numerical P-Δ curve computed from the FE model with a crack size of a_i. Since the crack size of the FE model equals the current crack size in the experimental specimen, the energy release rate calculated from the multiple FE specimens, using the same approach as the conventional multiple-specimen experimental approach, represents the J-value in the experimental specimen with the corresponding crack size.

The CMODs corresponding to the intersection points between the experimental curve and the numerical curves, *i.e.*, Δ_1 to Δ_n in Figure 1a, define the CMOD levels to compute the strain energy U for each crack depth. The evaluation of the strain energy U from the P-Δ curve becomes the primary step in applying the CMOD-based hybrid approach. Since the strain energy for the SE(B) specimen dissipates mainly through the rotation of the crack plane, the strain energy U equals the bending strain energy in the mode I SE(B) specimen. Based on the J-integral calculation proposed by Tohgo and Ishii [9], the bending strain energy for SE(B) specimen follows,

$$U_I = \int M d\theta \,. \tag{1}$$

Equation (1) also represents the mode I strain energy in mixed-mode I and II specimens. In such mixed-mode specimens, the shear strain energy follows,

$$U_{II} = \int F_V d\delta_V \,, \tag{2}$$

where, F_V is the shear force on the crack plane, and δ_V corresponds to the relative shear displacement between two crack planes. For the SE(B) specimens, the shear force remains zero and the bending moment M derives from equilibrium principles. The rotation of the crack plane, θ, depends on the current crack length,

$$\theta_i = \frac{\text{CMOD}}{a_{i-1} + r_p(W - a_{i-1})}, \tag{3}$$

where r_p represents the plastic rotation factor and equals 0.44 as suggested in ASTM E1820 [1] for SE(B) specimens, a_{i-1} corresponds to the crack depth determined at the previous intersection point between the experimental P-Δ curve and that obtained from the FE analysis, as demonstrated in Figure 1a.

Figure 1b illustrates the schematic variation of the strain energy with respect to the crack depth, calculated from multiple FE models. To facilitate the calculation of the energy release rate from the FE models, the hybrid approach utilizes a regression analysis to derive approximate polynomial functions in terms of the crack size, a, to describe the strain energy variations shown in Figure 1b. The solid circles in Figure 1b indicate the displacement level where the energy release rate calculated from multiple FE models equals (theoretically) the energy release rate in the experimental fracture specimen with a growing crack. The J-values at these solid circles are computed from Eq. (4),

$$J = -\frac{1}{B}\frac{dU}{da}. \tag{4}$$

Figure 1c sketches the J-values calculated at these solid circles with respect to the corresponding crack extensions. Tohgo and Ishii [9] separated the J-value for mixed-mode I and II specimens as,

$$J_T = J_I + J_{II} \,, \tag{5}$$

where, J_I and J_{II} correspond to the energy release rate contributed by the bending and shear deformation of the crack plane, respectively.

3. Validation on SE(B) Specimen

This section presents the validation of the proposed CMOD-based hybrid approach based on the

fracture resistance test results for the SE(B) specimens made of aluminum alloy (Al-alloy) 5083 H-112 reported by the authors [5]. The Al-alloy has a Young's modulus E of 69 GPa, with a Poisson's ratio of $\upsilon = 0.3$, the yield stress of $\sigma_y = 243$ MPa and the ultimate stress of $\sigma_u = 347$ MPa. Figure 2a presents the uniaxial stress-strain curves for the aluminum alloy material obtained from the axial tension test.

Figure 2a sketches the geometry of the SE(B) specimen. The total thickness of all the SE(B) specimen equals $B = 18$ mm, with the net-thickness after side-grooving equal to 80% of the total thickness, or $B_N = 0.8B$. The width of the specimen, W, equals to 36 mm, while the span over width, S/W, has a constant ratio of 4 for all SE(B) specimens. The CMOD or Δ is measured by the crack opening displacement gauge mounted at the mouth of the crack. The initial crack depth over the width ratios, a_0/W, equal 0.222 and 0.513 for the Al-alloy SE(B) specimens. The SE(B) specimen with a relatively shallow crack depth ($a_0/W \approx 0.2$) represents a fracture specimen with low crack-front constraints, while the deep crack ($a_0/W \approx 0.5$) corresponds to a high crack-front constraint condition complying with the ASTM E-1820 requirement [1].

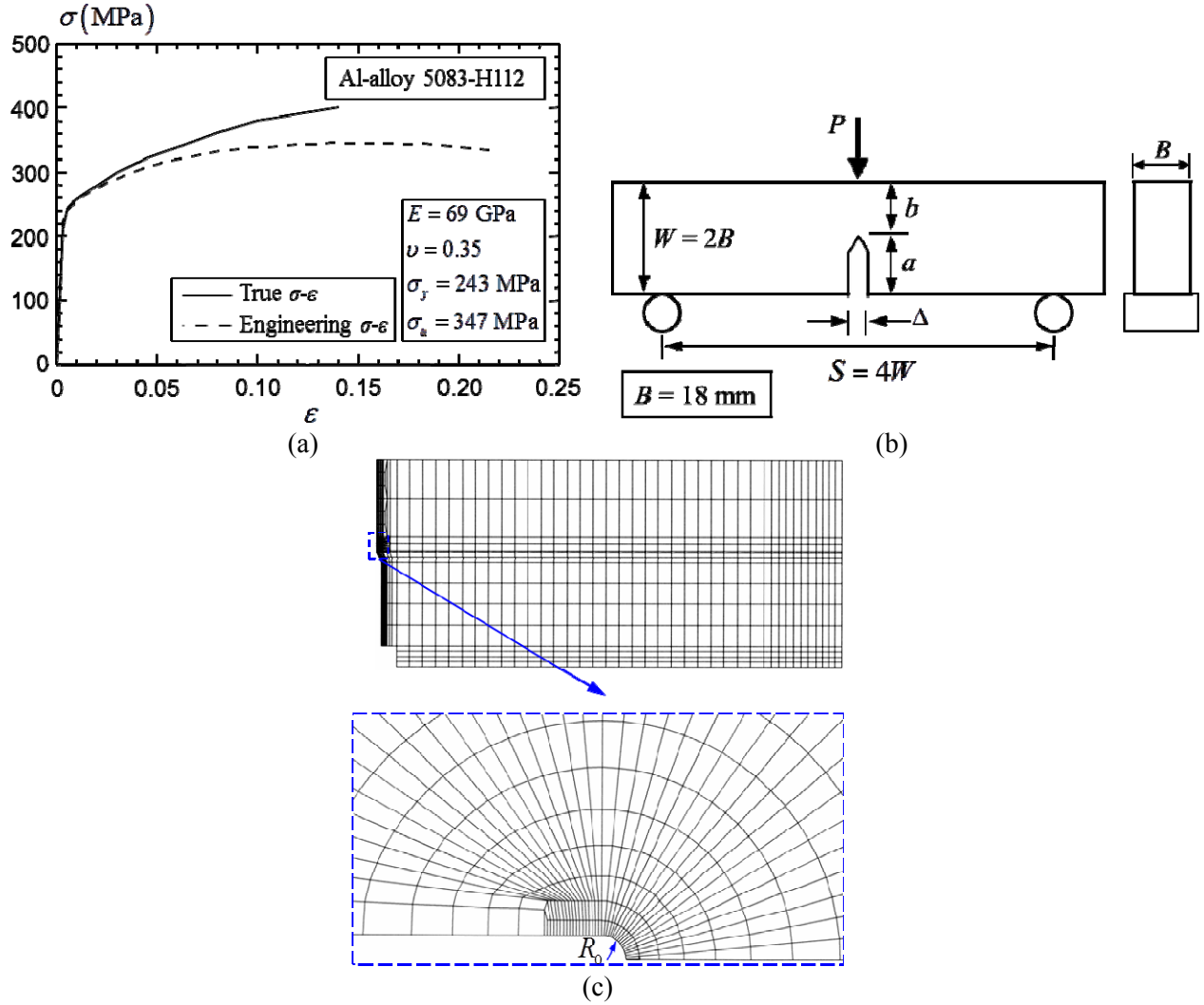

Figure 2. (a) Uniaxial stress-strain curves for the aluminum alloy material; (b) geometric configuration of the SE(B) specimen; and (c) the typical FE mesh for the SE(B) specimen.

Figure 2c shows a typical, half FE model for the Mode I SE(B) specimens, built from 3D 8-node brick elements. The FE model consists of one-layer of elements in the thickness direction, with all nodes in the FE model constrained against the out-of-plane displacement to represent the

plane-strain condition. The presence of a plane of symmetry enables a half model, with the displacement degree of freedom for all nodes on the plane of symmetry constrained in the direction normal to that plane. The crack-tip contains a focused mesh with an initial root radius of R_0 = 25 μm to facilitate numerical convergence under large deformations, as shown in Figure 2b. The total number of nodes in the FE models with different crack depths varies from 2000 to 3000, with the number of elements ranging from 1000 to 1500. The numerical computation in this study utilizes the FE research code, WARP3D [10].

For the Al-alloy SE(B) specimen with a_0/W = 0.222, this study generates thirteen FE models to compute the strain energy at thirteen different crack extensions (Δa_i), as summarized in Table 1. For the deep cracked SE(B) specimen with a_0/W = 0.511, the validation utilizes twelve FE models with various crack lengths to represent twelve different crack extensions (Δa_i), as shown in Table 1.

Table 1. The crack size in the FE models for the two SE(B) specimens made of Al-alloy 5083 H-112.

a_0/W	a_0 (mm)	Crack extensions (mm)					
		Δa_1	Δa_2	Δa_3	Δa_4 to Δa_{11}	Δa_{12}	Δa_{13}
0.222	8.0	0	0.2	0.5	1 to 4.5 @ 0.5 mm increment	5	5.5
0.511	18.5	0	0.2	0.6	1.2 to 5.4 @ 0.6 mm increment	6	-

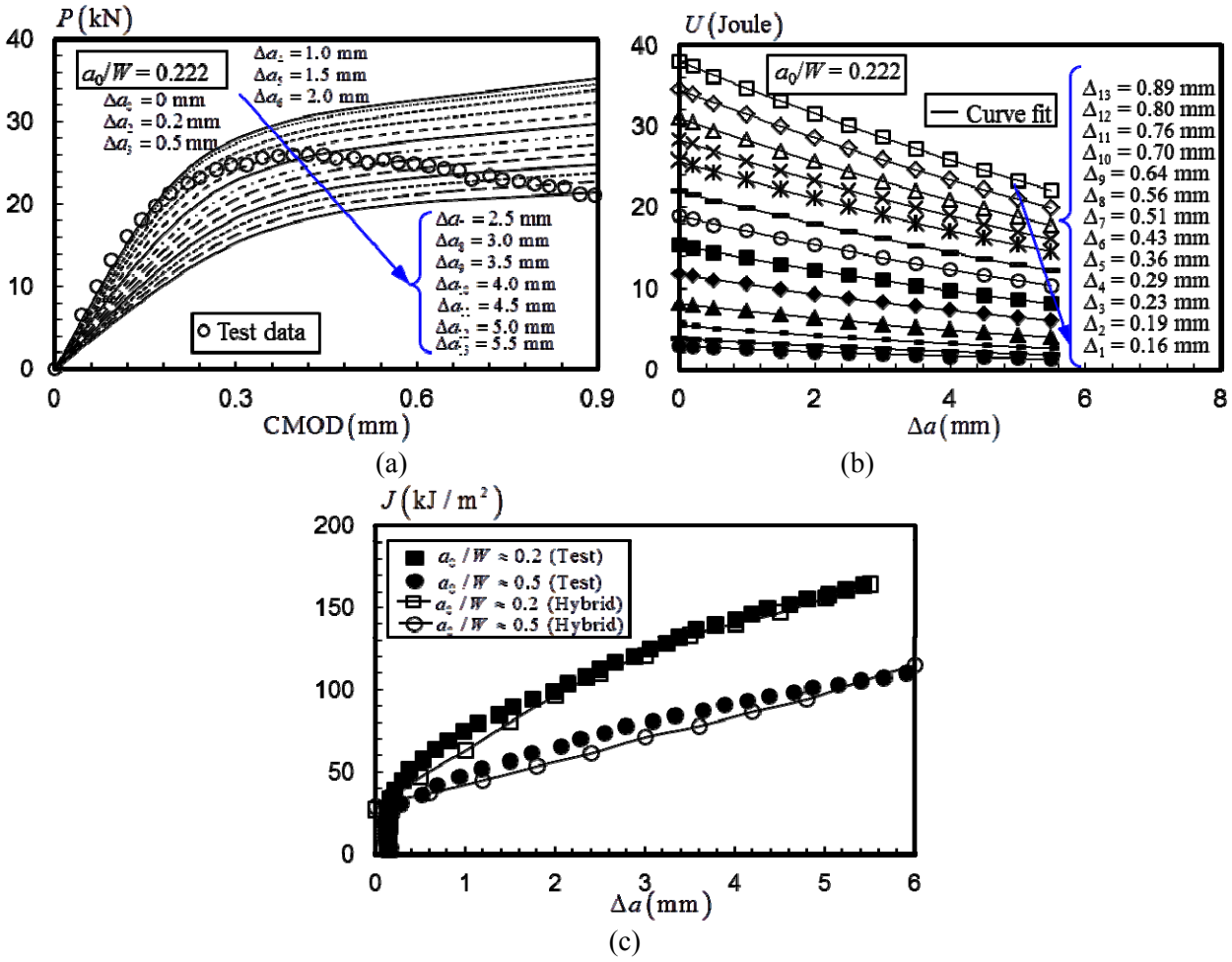

Figure 3. (a) P-Δ curve for SE(B) specimen with a_0/W=0.222; (b) U-Δa curves for SE(B) specimen with a_0/W=0.222; and (c) comparison of the J-R curves measured in the test and those derived from the CMOD-based hybrid approach for both shallow and deep cracked SE(B) specimens.

Figures 3a shows the P-Δ relationships for the experimental specimen of a_0/W = 0.222 with a growing crack indicated by the discrete circular symbols. The good agreement between the test data and the FE results at the zero crack extension, Δa = 0, confirms the boundary conditions of the FE models. In addition, the numerical P-Δ curve computed from the FE model with the same crack size as the experimental specimen at the end of the fracture test intersects with the test P-Δ curve at the end of the measured history. Figure 3b shows the strain energy U versus the crack extension evaluated from the P-Δ curves for the shallow cracked SE(B) specimen. The U value is computed at varied CMOD levels (Δ_i), which correspond to the intersections between the experimental and numerical P-Δ curves. The discrete symbols in Figure 3b represent the strain energy value computed from the FE model with the corresponding initial crack lengths $a_0+\Delta a_i$. The solid lines in Figure 3b correspond to the second-order polynomial functions derived from the regression analysis.

The J-value corresponding to each crack extension, Δa_i, can be derived from Eq. (4), using the first-order derivative of the fitted polynomial for the strain energy U (at the corresponding Δ_i) with respect to the crack depth. This leads to a J-R curve schematically shown in Figure 1c. The determination of the J-R curve by the CMOD-based hybrid approach for the SE(B) specimen with a_0/W = 0.511 follows the same procedures described in Figure 3a and 3b. Figure 3c compares the experimental J-R curves with those determined from the CMOD-based hybrid method for SE(B) specimens with two crack depth ratios, a_0/W = 0.222 and 0.511. The J-R curves obtained from the CMOD-based methods agree closely with the test results for both the shallow-crack and the deep-crack SE(B) specimens. This validates both the applicability and the accuracy of the CMOD-based hybrid method in determining the J-R curves for SE(B) specimens.

4. Validation on the Mixed-Mode Specimens

The verification of the hybrid method on the determination of the J-R curves utilizes two mixed-mode Al-alloy 5083 H-112 specimens reported by the authors [5, 11], the mode I dominant specimen AM1 (mode-mixity $\beta_{eq} = \tan^{-1}(K_I/K_{II}) = 75^o$) and the mode II dominant specimen AM5 ($\beta_{eq} = \tan^{-1}(K_I/K_{II}) = 20^o$) [5].

Figure 4a and 4b shows the typical FE models for the two mixed-mode specimens, AM1 and AM5. The geometrical configurations and the orientation of the crack planes follow exactly the test procedures described by the authors [5, 11]. Figure 4c and 4d illustrates the close-up view of the region around the crack tips for AM1 and AM5, respectively. The crack path deviates by 20^o from the original crack plane in the mode I dominant specimen AM1 and by 9^o from the original crack plane in the mode II dominant specimen AM5. The multiple FE models have varied crack lengths of $a_0+\Delta a_i$ along the crack directions observed from the tests, which have been summarized in Table 2. The verification of the CMOD-based hybrid approach on the mixed-mode specimens includes eight and six FE models with different crack sizes for the mode I dominant AM1 and the mode II dominant specimen AM5, respectively, as shown in Table 2. The crack tips for both specimens are simulated with an initial root radius of 25 μm to facilitate the convergence of the large-deformation analysis, similar to the method shown in the Figure 2c. The element type, boundary conditions and the calculation procedures follow similarly the methods described by Qian and Yang [7]. The material properties of the elements remain the same as those shown in Figure 2a.

Figure 5a and 5b show the M-θ curves and the F_V-δ_V relationships computed from the FE models listed in Table 2. The circles in Figure 5a and 5b represent the test results for AM1. Figure 5c and 5d illustrate the mode I strain energy U_I versus Δa curves and the mode II strain energy U_{II} versus Δa curves evaluated from the FE results at varied deformation levels listed in Table 2. The symbols

in Figure 5c and 5d represent the strain energy evaluated at different deformation levels (θ_i or δ_{Vi}) as listed in Table 2. The solid lines correspond to the fitted second-order polynomial functions, which are utilized to determine the first-order derivatives at various crack extensions.

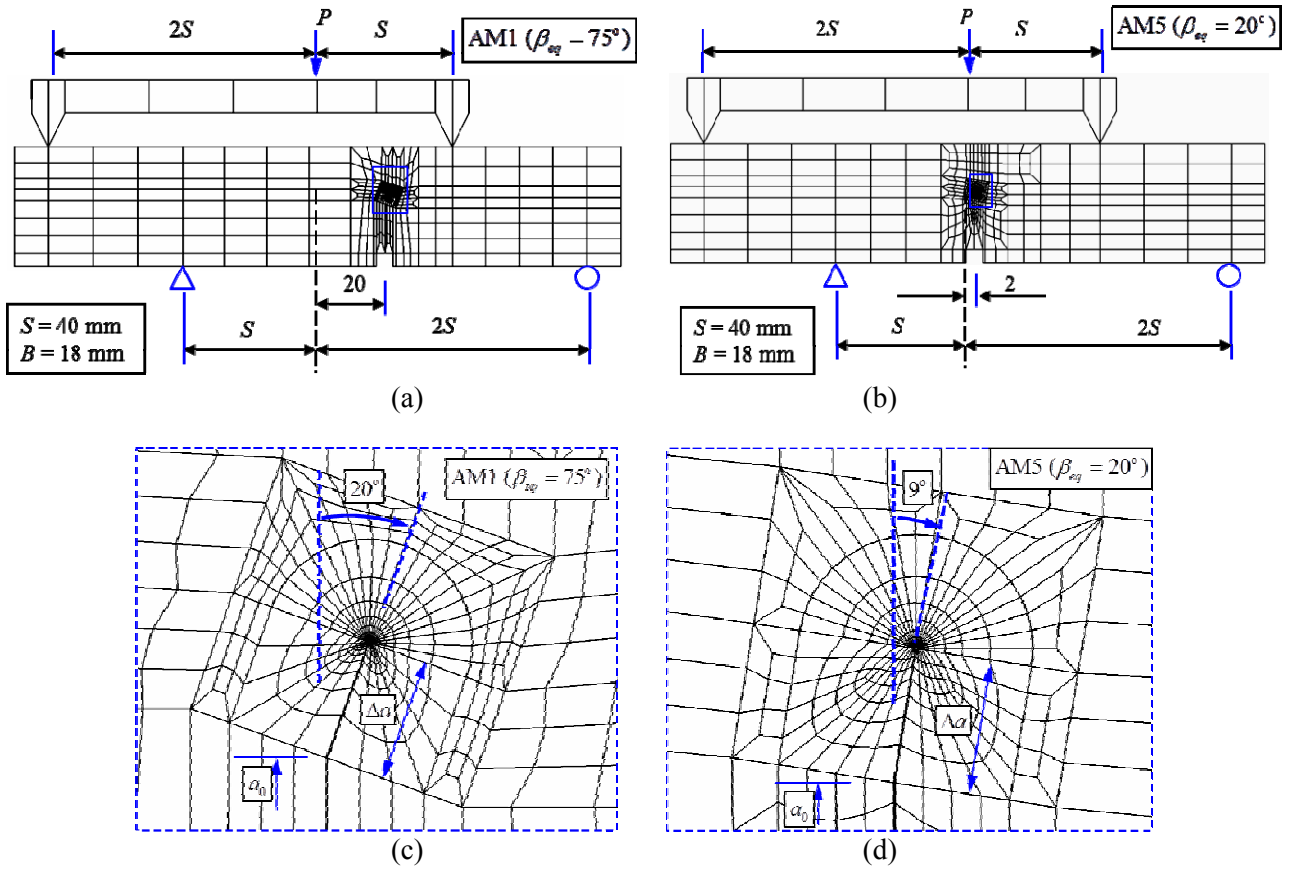

Figure 4. Typical FE models for the mixed-mode specimens made of Al-alloy 5083 H-112: (a) global FE model of the Mode I dominant specimen AM1; (b) global FE model of the Mode II dominant specimen AM5; (c) a close-up view around the crack tip for AM1; and (d) a close-up view around the crack tip for AM5.

Table 2. FE models for the mixed-mode I and II specimens made of Al-alloy 5083 H-112.

Specimen	Crack Parameters	FE models								
		$i = 0$	$i = 1$	$i = 2$	$i = 3$	$i = 4$	$i = 5$	$i = 6$	$i = 7$	$i = 8$
AM1 (Mode I dominant)	Δa (mm)	0	0.1	0.3	0.7	1.7	2.7	3.7	4.7	5.7
	θ (rad)	-	0.0247	0.0288	0.0356	0.06	0.0816	0.0924	0.106	0.115
	δ_V (mm)	-	0.052	0.09	0.159	0.273	0.486	0.588	0.672	0.749
AM5 (Mode II dominant)	Δa (mm)	0.15	0.5	1.0	2.0	3.0	3.9	4.5	-	-
	θ (rad)	-	0.017	0.019	0.021	0.022	0.023	0.024	-	-
	δ_V (mm)	-	0.604	0.731	0.911	1.050	1.233	1.412	-	-

Figure 6 compares the fracture resistance curves obtained from the hybrid approach and the test for AM1. Both the J_I-Δa and J_{II}-Δa hybrid results agree well with the test data at small crack extension, *i.e.*, $\Delta a < 1$ mm, as shown in Figure 6a. Figure 6a also shows that the hybrid approach leads to slightly lower J_I-Δa curve when $\Delta a > 1$ mm, due to the combined mode I dominant and mode II dominant fracture failure across the thickness of the specimen [11]. In general, the good agreement between the total J versus Δa curves determined using the hybrid approach and that obtained from

the test confirms the applicability of the hybrid method in predicting the fracture resistance for the Mode I dominant specimen AM1.

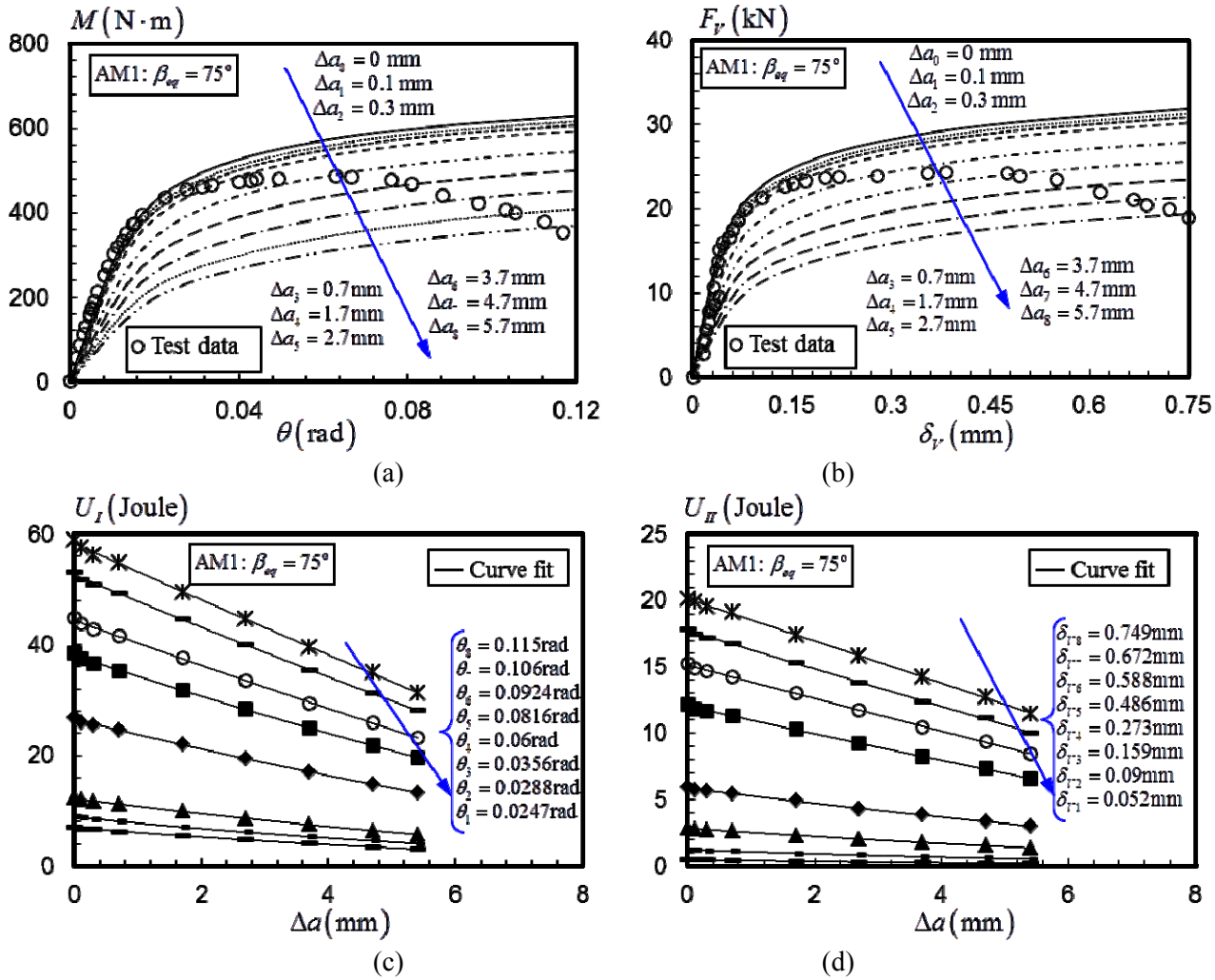

Figure 5. Determination of the strain energy for the Mode I dominant specimen, AM1: (a) The moment-rotation curves computed from multiple FE models; (b) the shear force versus shear deformation computed from multiple FE models; (c) the Mode I strain energy versus the change in the crack size; and (d) Mode II strain energy versus the change in the crack size.

Figures 6c and 6d compare the *J-R* curves reproduced from the hybrid approach and those obtained from the test for mode II dominant specimen, AM5. Very close agreement between the results obtained from these two methods is observed when $\Delta a < 1$ mm, as shown in Figure 6c and 6d. As $\Delta a > 1$ mm, the hybrid approach yields slightly lower (conservative) *J-R* curves.

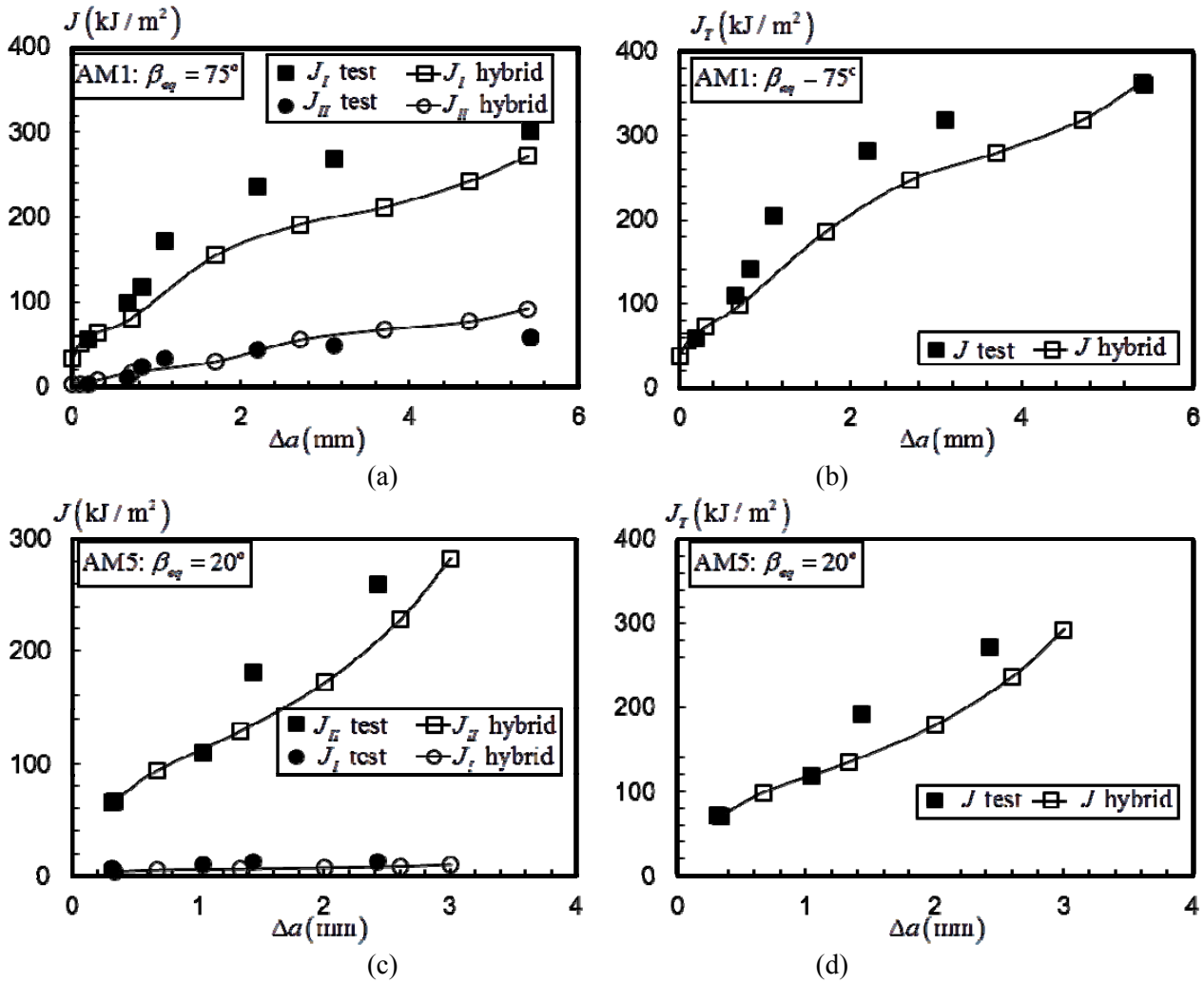

Figure 6. Verification for the mixed-mode specimen: (a) the Mode I and Mode II fracture toughness versus the crack extensions for AM1; (b) the total fracture toughness versus the crack extension curves for AM1; (c) the Mode I and Mode II fracture toughness versus the crack extensions for AM5; and (d) the total fracture toughness versus the crack extension curves for AM5.

5. Summary and Conclusions

The proposed CMOD-based hybrid method relies on a single experimental *P*-Δ curve and multiple numerical *P*-Δ curves to derive the fracture resistance curve for both the SE(B) specimen and the mixed-mode I and II specimen. The CMOD-based hybrid method simplifies the *J*-*R* curve testing procedure by eliminating the multiple unloading and reloading sequences, required to determine the specimen compliance and hence the crack size. The current CMOD-based hybrid method removes the dependence on the LLD, which requires careful instrumentation to prevent possible errors introduced by the indentation at the loading point. The close agreement between the *J*-*R* curves derived from the CMOD-based hybrid approach and those determined from the tests validates the proposed hybrid approach for both the SE(B) specimens and the mixed-mode I and II specimens.

References

[1] American Society for Testing and Materials, Standard test method for measurement of fracture toughness. ASTM E1820-11. West Conshohocken, PA, United States, 2011.
[2] International Standard Organization. Metallic Materials-Unified Method of Test for the

Determination of Quasistatic Fracture Toughness. International Standard ISO 12135, International Organization for Standardization, 2002.
[3] X. K. Zhu, J. A. Joyce, Revised incremental J-integral equations for ASTM E1820 using crack mouth opening displacement, J Test Eval, 37 (2009) 205-214.
[4] J. A. Joyce, Manual on elastic-plastic fracture: laboratory test procedures. West Conshohocken, PA, United States, American Society for Testing and Materials, 1996.
[5] X. Qian, W. Yang, Initiation of Ductile Fracture in Mixed-mode I and II Aluminium Alloy Specimens. Eng Fract Mech, 93 (2012) 189-203.
[6] J. A. Begley, J. D. Landes, The J-integral as a fracture criterion. ASTM STP 514 (1972) 1-20.
[7] X. Qian, W. Yang, A hybrid approach to determine fracture resistance for mode I and mixed mode I and II fracture specimens. Fatigue Fract Eng Mater Struct. 34 (2011) 305-320.
[8] X. Qian, W. Yang, A Hybrid Approach To Determine Ductile Fracture Resistance. Procedia Engineering. 10 (2011) 319-24.
[9] K. Tohgo, H. Ishii, Elastic plastic fracture-toughness test under mixed-mode I-II loading. Eng Fract Mech, 41 (1992) 529-40.
[10] A. Gullerud, K. Koppenhoefer, A. Roy, S. RoyChowdhury, M. Walters, B. Bichon, K. Cochran, A. Carlyle, R. H. Jr. Dodds. WARP3D: 3-D dynamic nonlinear fracture analysis of solids using parallel computers and workstations. Structural Research Series (SRS) 607 UILU-ENG-95-2012 University of Illinois at Urbana Champaign.
[11] W. Yang, X. Qian, The fracture resistance curve over the complete mixed-mode I and II range for aluminium alloys. Eng Fract Mech, 96 (2012) 209-225.